Supplementary Information (SI) for Nanoscale.

Supporting Information

Unveiling the underlying physical mechanisms of inverted perovskite solar cells

Long Fang[1,3], Yangang Zhang[1,3,], Chenyi Yang[1], Hengyue Li[2], Xiufen Ma[1], Wang Luo[1,3], Lina Liu[4], Yunfei Han[1*], Dongdong Zhang[1], Junliang Yang[2,*]*

[1] School of New Energy, Inner Mongolia University of Technology, Ordos 017000, China

[2] Hunan Key Laboratory for Super-microstructure and Ultrafast Process, School of Physics, Central South University, Changsha 410083, China

[3] College of Energy and Power Engineering, Inner Mongolia University of Technology, Hohhot 010051, China

[4] LONGi Green Energy Technology Co., Ltd., Ordos 017000, China

** Corresponding authors:*

junliang.yang@csu.edu;yfhan2017@sinano.ac.cn;13623830013@163.com.

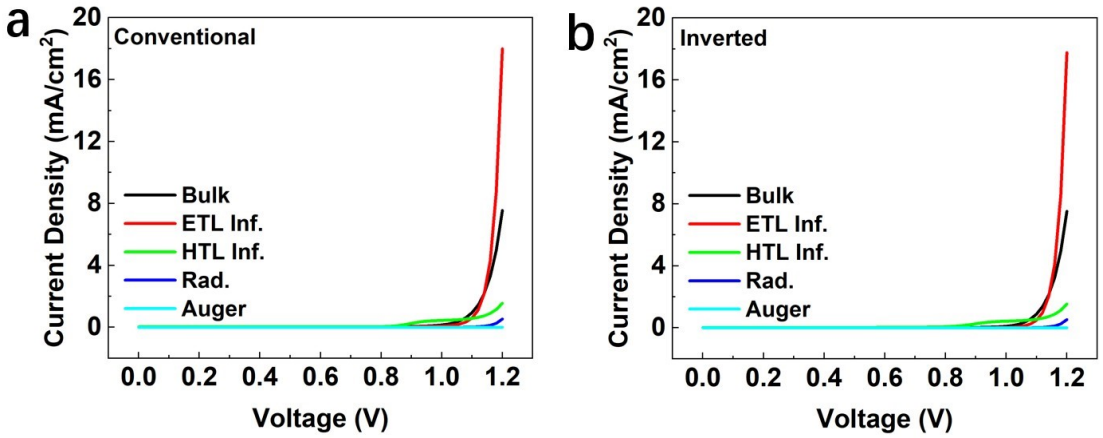

Figure S1. Current losses contributed from the different sources for (a) conventional and (b) inverted structure, respectively.

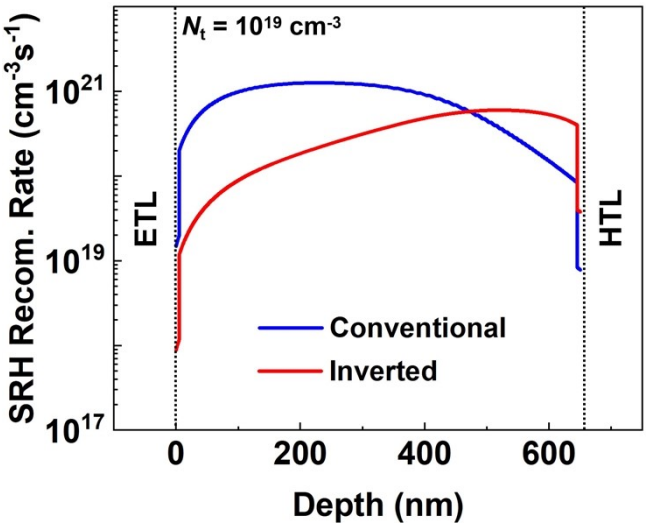

Figure S2. Spatial distribution of SRH recombination in conventional and inverted structures at N_t = 10^{19} cm^{-3}.

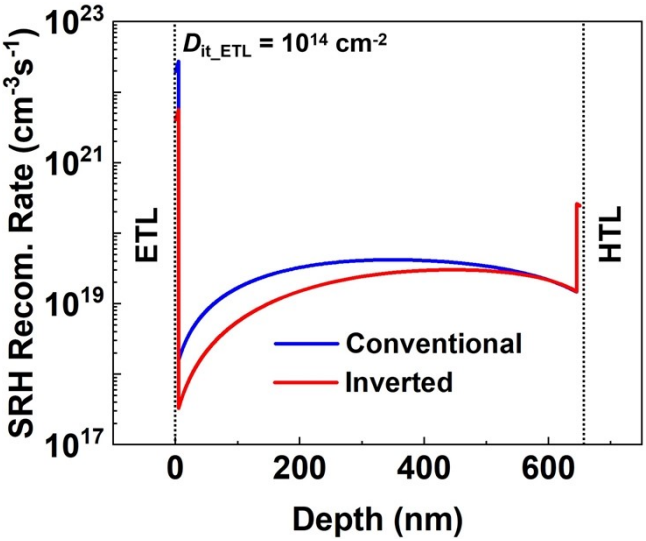

Figure S3. Spatial distribution of SRH recombination in conventional and inverted structures at D_{it_ETL} = 10^{14} cm^{-2}.

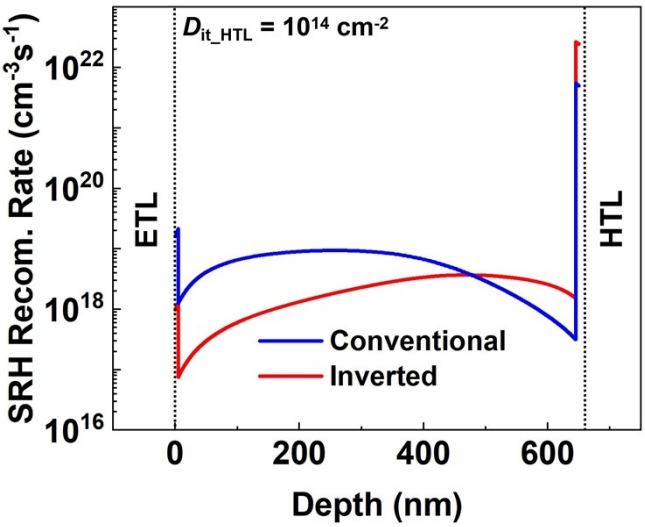

Figure S4. Spatial distribution of SRH recombination in conventional and inverted structures at D_{it_HTL} = 10^{14} cm^{-2}.

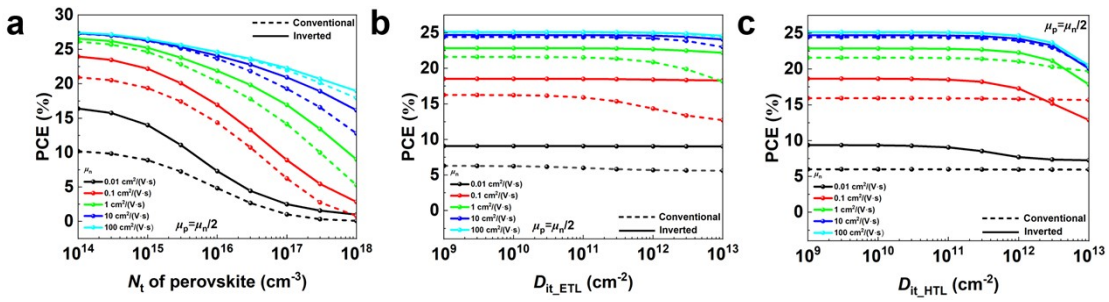

Figure S5 (a) Variation of PCE with N_t under different μ_n conditions; (b) Variation of PCE with D_{it_ETL} under different μ_n conditions; (c) Variation of PCE with D_{it_HTL} under different μ_n conditions. ($\mu_p=\mu_n/2$)[1]

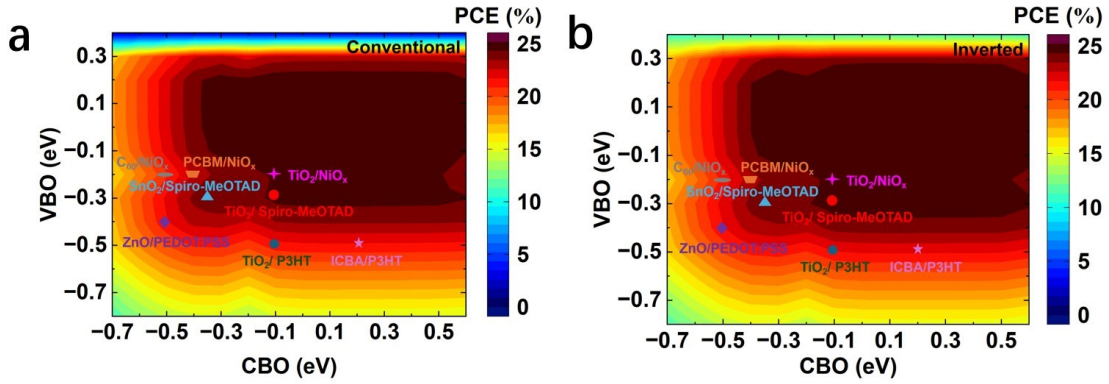

Figure S6. PCE as a function of VBO and CBO for (a) conventional structure and (b) inverted structure, respectively.

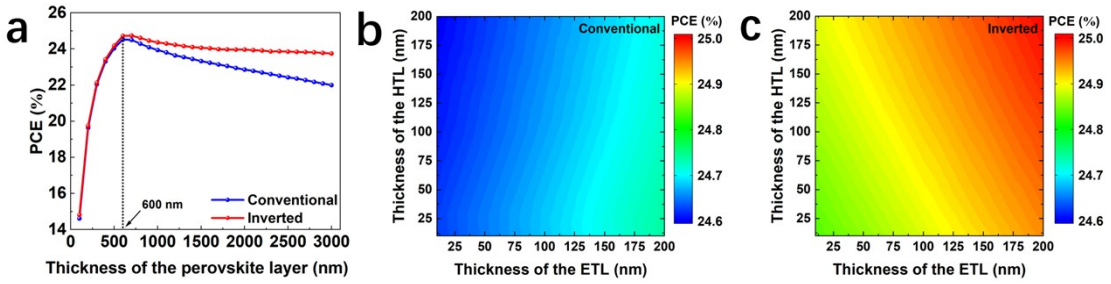

Figure S7. (a) PCE dependence on perovskite layer thickness for both conventional and inverted structures. (b) PCE versus transport layer thickness in the conventional structure. (c) PCE versus transport layer thickness in inverted structure.

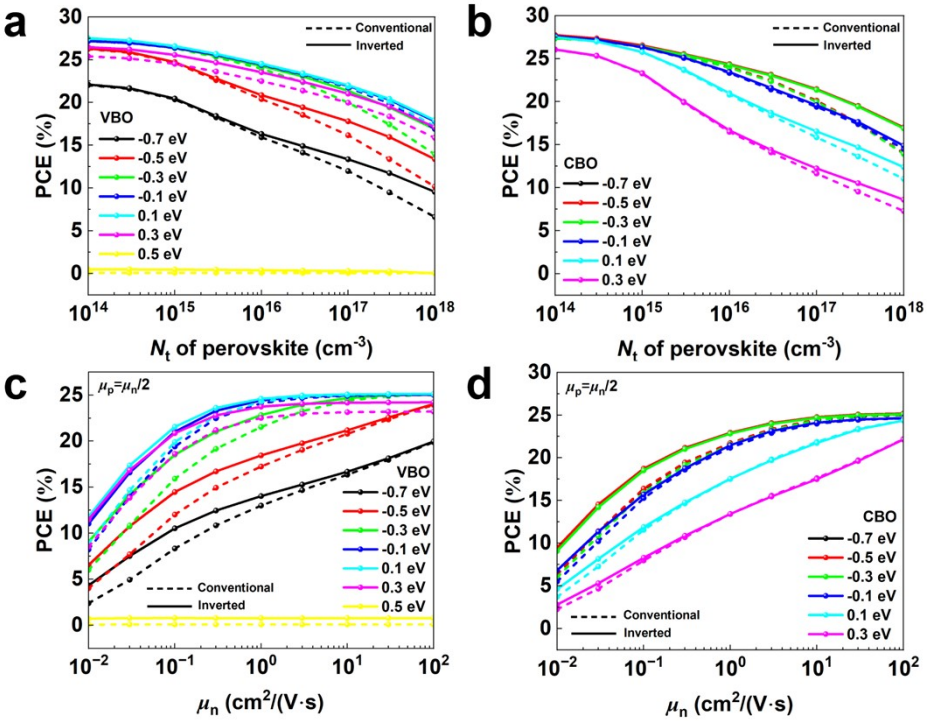

Figure S8 (a) Variation of PCE with N_t under different VBO conditions; (b) Variation of PCE with N_t under different CBO conditions; (c) Variation of PCE with μ_n under different VBO conditions; (d) Variation of PCE with μ_n under different CBO conditions. ($\mu_p=\mu_n/2$)[1]

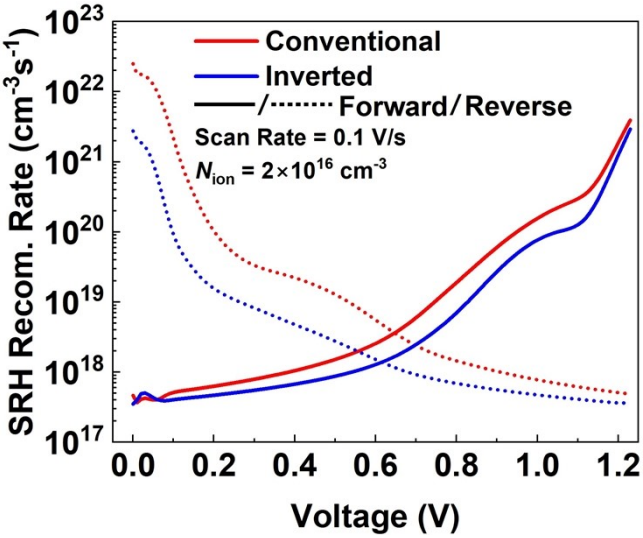

Figure S9. Average SRH recombination rates of conventional and inverted structures under forward/reverse voltage scans and different operating bias conditions.

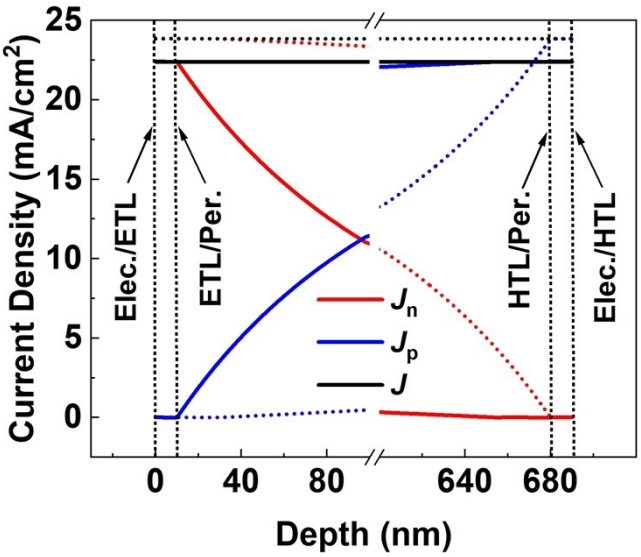

Figure S10. The distribution of electron current density (J_n), hole current density (J_p), and current density (J) in conventional and inverted structures.

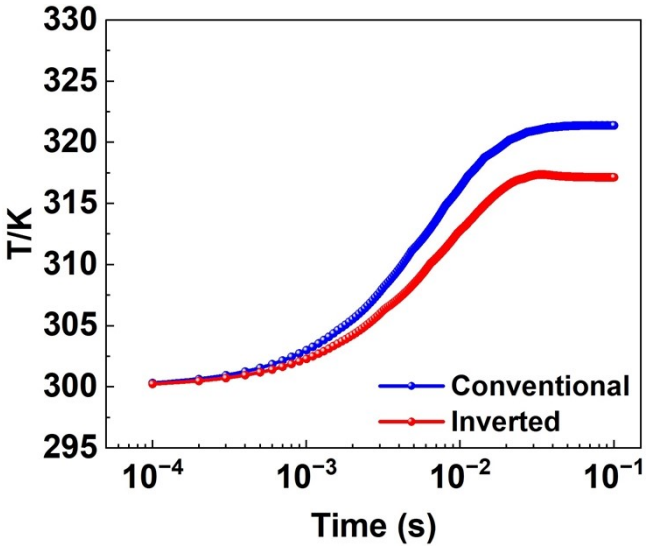

Figure S11. The variation of average device temperature with time at MPP.

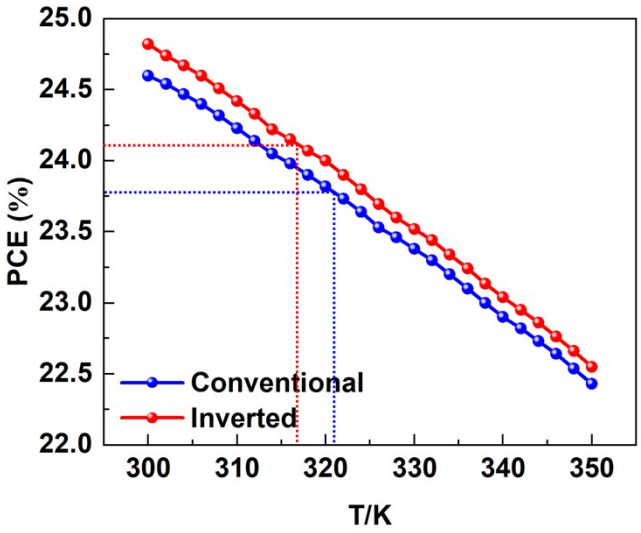

Figure S12. The variation of PCE of the two structures with temperature.

Table 1 Simulated input parameters of conventional structure[2-6]

Parameters	SnO_2	Perovskite	Spiro-MeOTAD
Thickness (nm)	10	650	30
Band gap (eV)	3.6	1.6	3
Electron affinity (eV)	4	3.9	2.2
Dielectric permittivity(relative)	9	6.5	3
Electron mobility (cm^2/Vs)	100	12.5	2.1×10^{-3}
Hole mobility (cm^2/Vs)	25	7.5	2.16×10^{-3}
Donor density-N_D (cm^{-3})	1.0×10^{18}	——	——
Acceptor density-N_A（cm^{-3}）	——	——	1×10^{18}
Total defeats density-N_t（cm^{-3}）	——	5.7×10^{15}	——
SRH recombination life [μs]	10	——	10
Radiative recombination coefficient, B_{rad} (cm^3s^{-1})	——	3.27×10^{-11}	——
Auger recombination coefficient, A_n/A_p (cm^6s^{-1})	——	0.88×10^{-29}	——
Density, ρ ($g\cdot cm^{-3}$)	3.8	4	1.2
conductivity,	2	0.01	0.3

($W \cdot m^{-1} \cdot K^{-1}$)			
Heat capacity ($J \cdot g^{-1} \cdot K^{-1}$)	0.7	0.5	0.2

Table 2 Simulated input parameters of inverted structure[2-6]

Parameters	Spiro-MeOTAD	Perovskite	SnO_2
Thickness (nm)	10	650	30
Band gap (eV)	3	1.6	3.6
Electron affinity (eV)	2.2	3.9	4
Dielectric permittivity(relative)	3	6.5	9
Electron mobility (cm^2/Vs)	2.1×10^{-3}	12.5	100
Hole mobility (cm^2/Vs)	2.16×10^{-3}	7.5	25
Donor density-N_D (cm^{-3})	——	——	1.0×10^{18}
Acceptor density-N_A（cm^{-3}）	1×10^{18}	——	——
Total defeats density-N_t（cm^{-3}）	——	5.7×10^{15}	——
SRH recombination life [μs]	10	——	10
Radiative recombination coefficient, B_{rad} (cm^3s^{-1})	——	3.27×10^{-11}	——
Auger recombination coefficient, A_n/A_p (cm^6s^{-1})	——	0.88×10^{-29}	——
Density, ρ ($g\cdot cm^{-3}$)	1.2	4	3.8

conductivity, ($W \cdot m^{-1} \cdot K^{-1}$)	0.3	0.01	2
Heat capacity ($J \cdot g^{-1} \cdot K^{-1}$)	0.2	0.5	0.7

Reference：

[1] Z. Yang, W. Yang, X. Yang, J. C. Greer, J. Sheng, B. Yan and J. Ye, Device physics of back-contact perovskite solar cells, *Energy Environ. Sci.*, 2020, **13**, 1753-1765.

[2] M. K. Hossain, G. F. I. Toki, A. Kuddus, M. H. K. Rubel, M. M. Hossain, H. Bencherif, M. F. Rahman, M. R. Islam and M. Mushtaq, An extensive study on multiple ETL and HTL layers to design and simulation of high-performance lead-free $CsSnCl_3$-based perovskite solar cells, *Sci Rep*, 2023, **13**, 2521.

[3] Y. Zhang, Y. Bao, Y. Zhao, T. Ma, L. Shi, C. Zhang, Z. Ai, Y. Zhan, L. Qin, C. Wang, G. Cao, X. Li and Z. Yang, Tracing the Energy Losses in All-Perovskite Tandem Solar Cells From Opto-Electro-Thermal Perspectives, *Adv. Funct. Mater.*, 2025, 2503408.

[4] Z. Ai, T. Ma, Y. Zhang, Y. Bao, L. Shi, Z. Yang, Y. Zhan, L. Qin, G. Cao and X. Li, Unveiling Energy Conversion Mechanisms and Regulation Strategies in Perovskite Solar Cells, *Small*, 2024, **20**, e2404012.

[5] Y. Liu, L. Zheng, K. Zhang, K. Xu, W. Xie, J. Zhang, Y. Tian, T. Liu, H. Xu, R. Ma, W. Huang, J. Chen, J. Bao, C. Chen, Y. Zhou, X. Wang, J. Chen and J. Wang, Enhancing the crystallinity and stability of perovskite solar cells with 4-tert-butylpyridine induction for efficiency exceeding 24%, *J. Energy Chem.*, 2024, **93**, 1-7.

[6] Y. Zhang, Z. Yang, T. Ma, Z. Ai, Y. Bao, L. Shi, L. Qin, G. Cao, C. Wang and X. Li, Device Physics and Design Principles of Mixed-Dimensional Heterojunction Perovskite Solar Cells, *Small Sci.*, 2024, **4**, 3, 2300188.